J. Membrane Biol. 159, 113–125 (1997)

The Journal of
Membrane
Biology

A Kinetic Model with Ordered Cytoplasmic Dissociation for SUC1, an *Arabidopsis* H^+/Sucrose Cotransporter Expressed in *Xenopus* Oocytes

J.-J. Zhou,[1] **F. Theodoulou,**[1] **N. Sauer,**[2] **D. Sanders,**[3] **A.J. Miller**[1]

[1]Biochemistry and Physiology Department, IACR-Rothamsted, Harpenden, Hertfordshire, AL5 2JQ, UK
[2]Lehrstuhl Botanik II, University of Erlangen-Nürnberg, Staudtstraße 5, D-91058 Erlangen, Germany
[3]The Plant Laboratory, Biology Department, University of York, PO Box 373, York, YO1 5YW, UK

Received: 23 January 1996/Revised: 16 April 1997

Abstract. To elucidate the kinetic properties of the *Arabidopsis* H^+/sucrose cotransporter, SUC1, with respect to transmembrane voltage and ligand concentrations, the transport system was heterologously expressed in *Xenopus laevis* oocytes. Steady-state plasma membrane currents associated with transport of sucrose were measured with two-electrode voltage clamp over the voltage range −180 to +40 mV as a function of extracellular pH and sugar concentrations. At any given voltage, currents exhibited hyperbolic kinetics with respect to extracellular H^+ and sugar concentrations, and this enabled determination of values for the maximum currents in the presence of each ligand (i^H_{max}, i^S_{max} for H^+ and sucrose) and of the ligand concentrations eliciting half-maximal currents (K^H_m, K^S_m). *The* i^H_{max} and i^S_{max} exhibited marked and statistically significant increases as a function of increasingly negative membrane potential. However, the K^H_m and K^S_m decreased with increasingly negative membrane potential. Furthermore, at any given voltage, i^S_{max} increased and K^S_m decreased as a function of the external H^+ concentration. Eight six-state carrier models—which comprised the four possible permutations of intracellular and extracellular ligand binding order, each with charge translocation on the sugar-loaded or -unloaded forms of the carrier—were analyzed algebraically with respect to their competence to account for the ensemble of kinetic observations. Of these, two models (first-on, first-off and last-on, first-off with respect to sucrose binding as it passes from outside to inside the cell and with charge translocation on the loaded form of the carrier) exhibit sufficient kinetic flexibility to describe the observations. Combining these two, a single model emerges in which the binding on the external side can be random, but it can only be ordered on the inside, with the sugar dissociating before the proton.

Key words: H^+/sucrose cotransport — Electrogenic cotransporter — Steady-state — Kinetics — *Xenopus* oocytes — *Arabidopsis thaliana* — Kinetic modelling

Introduction

Although green plants are autotrophic, and synthesize carbohydrates via photosynthesis, they possess heterotrophic tissues and organs (sinks), which are dependent on import of carbohydrates from autotrophic source tissues. The redistribution of carbohydrates within the plant, usually occurs in the form of sucrose, via the phloem transport system (Frommer & Sonnewald, 1995). The transport of sucrose into the phloem has been shown to be energy-dependent and proton-linked (Komor et al., 1977). Sucrose transport across the plasma membrane can be energized by symport with H^+, with the driving force provided by the transmembrane pmf set up by the H^+-pumping ATPase (*see* reviews by Reinhold & Kaplan, 1984, Bush, 1993).

A sucrose carrier from spinach leaf was isolated using complementation cloning of *Saccharomyces cerevisiae* (Riesmeier et al., 1992). The strain was engineered to express a cytoplasmic form of yeast invertase, which then allowed cells which were expressing a sucrose carrier to grow when the only carbon source was sucrose. The spinach cDNA was then used to probe an *Arabidopsis thaliana* library and to isolate two related sucrose

Correspondence to: A.J. Miller

Abbreviations: DEPC: diethyl pyrocarbonate; HEPES: (N-[2-hydroxyethyl]piperazine-N′-[2-ethylsulfonic acid]); MBS: modified Barth's saline; MES: (2-[N-morpholino]ethanesulfonic acid)

transporters, SUC1 and SUC2 (Sauer & Stolz, 1994). Yeast cells transformed with *SUC1* were able to accumulate the ^{14}C-labeled sucrose, whereas cells transformed with the gene in antisense orientation were not (Sauer & Stolz, 1994). Furthermore, this uptake was shown to be pH-dependent with uptake increasing with proton concentration but saturating between pH 5 and 6.

Cloning plant transporters has enabled electrophysiological characterization by heterologous expression in *Xenopus laevis* oocytes (Boorer et al., 1992, 1994). The application of voltage clamp techniques to oocytes permits transporter-mediated currents to be assayed as a function of membrane potential. This opens an extra dimension to analysis of the kinetic behavior of the transporter because, for these transporters which are electrophoretic, the membrane potential is a component of the driving force and is normally uncontrolled in radiometric assays of substrate uptake. Steady-state and presteady-state currents associated with a plant hexose transporter activity in *Xenopus* oocytes have been measured and a range of kinetic parameters quantified (Boorer et al., 1994).

In principle, the ligand binding order and identity of the charge-translocation reaction (i.e., on the loaded or unloaded carrier) can be discerned from the kinetic properties of an ion-coupled transport system, providing sufficient kinetic detail is available (Sanders et al., 1984). In the present study, we have expressed *SUC1* in oocytes to determine its kinetic response to changes in the external concentration of both ligands (sucrose and H^+) and to membrane voltage. The results have been subjected to analysis without preconceptions with respect to ligand binding order or to identity of the charge translocation reaction in an attempt to derive a kinetic model which is uniquely compatible with the data. This is the first rigorous analysis of binding order in a cloned H^+-driven cotransporter. We demonstrate that two such models are competent in describing the kinetics of SUC1-mediated currents in all the conditions we study, but that one of these models — first-on first-off with respect to sucrose, and with charge translocation on the loaded form of the carrier — fits better than the other. Nonetheless, combining these two, a single model emerges in which the binding on the external side can be random, but it can only be ordered on the inside, with the sugar dissociating before the proton.

Materials and Methods

Oocyte and cRNA Preparation

A full-length cDNA for the *Arabidopsis thaliana* SUC1 H^+/sucrose cotransporter (pTF2011) was subcloned into the *Eco* RI site of pBluescript SK− (Stratagene, Cambridge, UK). The resulting construct, pSUC1/BS, was linearized by digestion with *Not* I, and cRNA was transcribed and capped using an Ambion T3 mRNA mMachine™ (AMS Biotechnology, Oxford, UK) in vitro transcription kit according to the manufacturers instructions.

Oocytes were removed by surgery from adult *Xenopus laevis* females (Blades Biological, Edenbridge, Kent, UK), and washed in Modified Barth's Saline (MBS in mM: 88 NaCl, 1 KCl, 0.82 $MgSO_4$, 0.41 $CaCl_2$, 0.33 KNO_3, 2.4 $NaHCO_3$, 15 HEPES-NaOH pH 7.6) supplemented with streptomycin and penicillin, both at 10 μg/ml. The ovarian lobes were dissected into small clumps and treated with 2 mg/ml of collagenase (Sigma type 1A) in MBS for 1–2 hr at room temperature. Oocytes were washed thoroughly with MBS and stored overnight at 18°C. Stage V or VI oocytes (Dumont, 1972) were chosen for injection with 50 nl SUC1 cRNA (1 μg/μl), or 50 nl DEPC treated water. Experiments were performed 3–4 days after cRNA injection.

Electrophysiology

Oocyte currents were measured using the two microelectrode voltage-clamp method. Both electrodes were filled with 3 M potassium acetate and 20 mM KCl solution with resistances ranging from 0.5 to 2 MΩ. For all electrophysiological measurements, a simple frog saline containing (in mM): 115 NaCl, 2.5 KCl, 1.8 $CaCl_2$, 10 HEPES, pH 7.2 was used. For more acidic frog salines, MES was added in place of HEPES; the pH was adjusted by the addition of NaOH solution. Experiments were performed in a 0.5 ml Plexiglass chamber perfused continuously with normal Ringer solution at a rate of 2 ml/min. Oocytes were impaled with the voltage electrode and the membrane potential allowed to stabilize for 10–15 min before the current electrode was inserted. Only oocytes which had resting potentials more negative than −30 mV in normal frog saline at pH 7.2 were used in voltage-clamp experiments. Each experiment was performed at least twice using oocytes from four different animals. Voltage clamp was performed using an OOC-1 Dual Electrode Voltage Clamp (World Precision Instruments). Current-voltage (*I-V*) relations were obtained with a pulse protocol generated by a 486 computer via a Labmaster DMA A/D interface using the pCLAMP software 5.5 (Axon Instruments, Foster City, CA). The oocyte membrane potential was clamped at a holding potential of −80 mV from which the membrane was pulsed for 120 msec in a bipolar staircase to the test potentials between −180 to 40 mV with 20 mV increments, followed by a 1-sec interpulse interval at the holding potential. In all experiments, the oocytes were allowed to adjust for at least five min after changing the external pH before any sugar treatments were applied. Exposure to sugar was for less than 1 min, to minimize the accumulation of sugar within the cell. The *I-V* relationships were constructed from the steady-state currents, and data were only accepted when before and after *I-V* profiles were identical. Sucrose-dependent currents were obtained by subtracting the currents measured before from those obtained after the addition of the sugar. At any given membrane potential, steady-state sucrose-dependent currents measured as a function of external ligand concentration (i.e., either H^+ or sucrose) were filtered to Eq. 1 by a non-weighted, nonlinear least squares method using the SigmaPlot software (Jandel Scientific, Germany);

$$i = i_{max}[\text{substrate}]^n/\{[\text{substrate}]^n + (K_m)^n\} \quad (1)$$

where the substrate is either sucrose or H^+ and n is the coupling coefficient. These fits yielded the maximal currents i^H_{max} for H^+ and i^S_{max} for sucrose, and the half maximal ligand concentrations K^H_m (at saturating sucrose concentration) and K^S_m (at saturating H^+ concentration) respectively (Parent et al., 1992*a*).

Algebraic Analysis of Models

Carrier Model Topology and General Definitions — Eight simple ordered binding models were considered. These comprised the four dif-

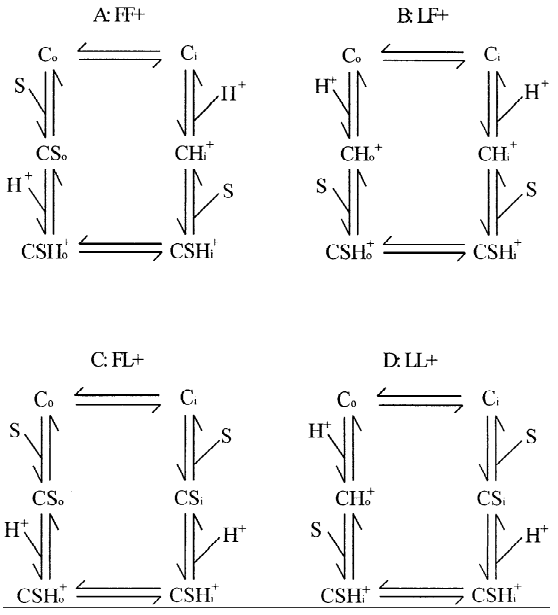

Fig. 1. Hypothetical simple ordered-binding models for SUC1. These models are defined by the order of sucrose binding. (*A*) First-on first-off, (FF). (*B*) Last-on first-off, (LF). (*C*) First-on last-off, (FL). (*D*) Last-on last-off, (LL). For clarity of presentation only the models in which the loaded carrier has a net positive charge are shown, but the four possible models in which the unloaded carrier has a net negative charge were also considered in the analysis of SUC1 kinetics.

ferent permutations of binding order for sucrose (S) (*see* Fig. 1), each with the possibility of charge translocation either on the sugar-loaded or unloaded form of the carrier. In accord with the notations used in previous analyses (e.g., Sanders et al., 1984) the models are described with respect to binding order of the sugar as it passes from outside to inside the cell. Likewise, if charge translocation is on the sugar-loaded form of the carrier then positive charge will be carried into the cell (+ models) whereas charge translocation on the unloaded form of the carrier will involve movement of negative charge out of the cells (− models); thus by this notation the model shown in Fig. 1*A* is first-on, first-off positive model (FF+) with respect to S; LF+, FL+ and LL+ models are shown in Fig. 1*B–D*, respectively. For all eight models, coupling between H^+ and S is assumed to be tight: there is no slip pathway envisaged for the uncoupled translocation of S (*cf.* Parent et al., 1992*a*). This appears reasonable because the presence of a quantitatively significant slip pathway would lead to dissipation of the sugar gradient generated by H^+-coupling and is supported by the previous analysis of the Na^+-coupled mammalian sugar transporter SGLT1 expressed in *Xenopus* oocytes in which the slip pathway was shown to be negligible (Parent et al., 1992*a*).

Each of the carrier states in the reaction kinetic models can be represented by the general scheme in Fig. 2 with the unidirectional rate constants defined as shown. Ligand concentrations are subsumed within the rate constants k_{53}, k_{31}, k_{64} and k_{42}, although the actual identity of the ligand which binds is model-dependent. If ligand concentration is one of the experimental variables and it is necessary to make the ligand concentration explicit, then the rate constants are expanded as, for example, in the FL model, $k_{53} = k^o_{53}[S]_o$. Thus, the zero superscripts effectively indicate the value of the rate constant at a ligand concentration of 1 M.

The effect of membrane voltage can be incorporated into the

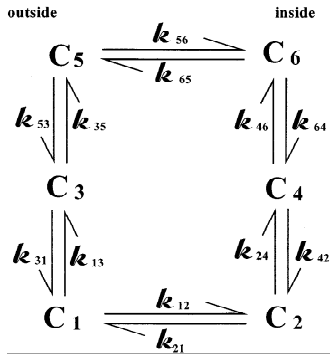

Fig. 2. General six-state ordered-binding model for SUC1 showing the rate constants for each step.

charge translocation reactions using an Eyring barrier (Hansen et al., 1981). For the + models in which k_{12} and k_{21} are the voltage-sensitive reactions we can write

$$k_{12} = k^o_{12}\exp(-zu\delta) \tag{2a}$$

and

$$k_{21} = k^o_{21}\exp(zu\{1-\delta\}), \tag{2b}$$

in which k^o_{12} and k^o_{21} are the rate constants at zero voltage, z is the net charge which is translocated, δ is the fractional distance of the energy barrier across the membrane from the outside and u is the reduced membrane potential, defined as FV_m/RT where V_m is the membrane potential in volts and R, T and F have their usual meanings. Similarly for the − models,

$$k_{65} = k^o_{65}\exp(zu\{1-\delta\}) \tag{3a}$$

and

$$k_{56} = k^o_{56}\exp(-zu\delta). \tag{3b}$$

The current through the + models is given as

$$i_+ = C_t zF([CSH_{i2^+}/C_t]k_{21} - [CSH_o{}^+/C_t]k_{12}) \tag{4a}$$

and through the − models as

$$i_- = C_t zF([C_i^-/C_t]k_{65} - [C_o^-/C_t]k_{56}), \tag{4b}$$

where C_t is the total carrier density in the membrane (units mol.m^{-2}) and the square bracketed terms are the fractional steady-state concentrations of the respective carrier species (binding sites inward- or outward-facing, bound or unbound).

General Rate Equations

Using the approach of King and Altman (1956), each of the terms in square brackets in Eqs. 4 can be expressed solely in terms of the component rate constants of the carrier cycle, thereby permitting the carrier-mediated current to be described as a function both of ligand concentration and of voltage.

One simplification to the general rate equations can be achieved at the outset. If the intracellular sucrose concentration of *Xenopus* oocytes is sufficiently low so that it has no impact on the kinetics, k_{64}

can be set to zero in the case of the FL and LL models, and k_{42} set to zero in the FF and LF models. In support of this simplification we have found that magnitude of SUC1-mediated currents was not changed by incubating an oocyte in sucrose for 10 min (*data not shown*) suggesting that sucrose accumulation within the oocyte does not have any significant effect.

Applying the King-Altman approach together with the simplification above yields the following expansion of Eqs. 4 for both the + and − models:

$$i = N \cdot (-k_{12}k_{24}k_{46}k_{65}k_{53}k_{31}/DEN) \tag{5}$$

in which the H^+:sucrose coupling ratio is taken as 1:1 (this is supported by the results shown in Fig. 10) with resultant values of $z = +1$ (+ models) and −1 (− models), N ($= C_t \cdot F$) is a scaling factor, and *DEN* is a denominator which comprises the sum of 21 terms each of which is the product of 5 rate constants. The exact identity of these 21 terms will depend on which order the ligands dissociate from the carrier on the inside because the simplification relating to the low intracellular sucrose concentration eliminates the terms containing *either* k_{64}− *or* k_{42}, depending on the model. The terms comprising *DEN* are shown in the left hand column of Table 1.

It will be noted that the numerator of Eq. 5 includes rate constants which subsume membrane potential (k_{12}, + models; k_{65}, − models), $[S]_o$(k_{53}, FL and FF models; k_{31}, LF and LL models) and $[H^+]_o$ (k_{31}, FL and FF models; k_{53}, LF and LL models). Thus, the numerator is sensitive to any of the three experimental variables, regardless of which model actually applies. By contrast, as shown in Table 1, for any given model the denominator contains some terms subsuming individual ligands, and some which do not. For example, of the 21 terms in the denominator of Eq. 5 as it applies to the FL+ model, 11 subsume $[S]_o$, 9 subsume $[H^+]_o$ and 17 subsume V_m.

These general properties mean that with respect to either of the external ligands, and for any of the eight models, we can rewrite Eq. 5 as

$$i = \frac{-Ak^o[L]_o}{Bk^o[L_o] + C} \tag{6}$$

where $[L]_o$ is the external concentration of ligand (either H^+ or sucrose), A is the product of N and the ligand-independent rate constants in the numerator of Eq. 5, k^o is the ligand-dependent rate constant with $[L]_o$ extracted (either k^o_{53} or k^o_{31}), B is the sum of the ligand-dependent terms in *DEN* with $k^o[L]_o$ extracted and C is the sum of the ligand-independent terms in *DEN*. By dividing both numerator and denominator of Eq. 6 by Bk^o, the equation can be re-cast in Michaelis-Menten format as

$$i = \frac{-i^L_{max}[L]_o}{[L_o] + K^L_m} \tag{7}$$

in which i^L_{max} is formally defined as (A/B) and K^L_m as (C/Bk^o), both from Eq. 6.

Just as terms can be grouped in the denominator of Eq. 5 into those that do and do not subsume $[L]_o$ to yield the denominator of Eq. 6, so the terms which define the Michaelis parameters (i^L_{max}, K^L_m) can be grouped according to whether or not they subsume the alternative ligand concentration ($[L']_o$). For all models and for either i^S_{max} or i^H_{max} the relationships have the form

$$i^L_{max} = \frac{[L']_o{}^a}{[L']_o{}^{b+c}} \tag{8}$$

while the expression for the K_ms is universally

$$K^L_m = \frac{[L']_o{}^{d+e}}{[L']_o{}^{b+c}} \tag{9}$$

with the coefficients a through to e representing grouped terms characteristics of each model. Expressed as a function of V_m, the i_{max} terms exhibit a similar pattern of a single voltage-dependent term in the numerator and both voltage-dependent and -independent terms in the denominator, while for the K_m terms the numerator can, depending on the model, comprise solely voltage-dependent terms or voltage-independent terms too. For each model, then, each of the parameters i^S_{max} and K^S_m, i^H_{max} and K^H_m can be expressed as a function of the elementary rate constants. Also, for each of the Michaelis parameters, such relationships can be cast in a format which makes explicit the response to either of the other two experimental variables (i.e., the other ligand, and V_m). Thus, each model can be characterized algebraically in terms of eight separate responses which can be subjected to experimental test.

Strategy for Derivation of a Kinetic Model for SUC1

The foregoing analysis demonstrates that each of the eight kinetic models can exhibit considerable kinetic flexibility. Such flexibility is problematic in the context of ascertaining whether a single model is uniquely competent in its ability to describe the observed kinetics of current flow through SUC1. Two solutions to this problem have been recommended previously (Sanders & Hansen, 1981; Sanders et al., 1984), and are utilized in the present study.

First the array of algebraically defined parameters can be subjected to experimental scrutiny using a ''brute force'' approach. This involves assaying the kinetic response of the SUC1-mediated currents over a range of conditions. A given kinetic response in one set of conditions must imply a particular size-ordering of the rate constants embedded within the coefficients a through to e in Eqs. 8 and 9 (and congeners in the case of a response to V_m). For example, if there is an observed increase in both i^S_{max} and K^S_m in response to an increase in $[H^+]_o$, then Eqs. 8 and 9 imply $c > b$ and $d > e$. Some of the individual rate constants embedded selectively in the coefficients can then be assigned relative values for each of the eight models to replicate the experimental behavior. For each model, this conditional size-ordering can then be applied to simplify the expended forms of Eqs. 8 and 9, and the equations then tested for their capacity to describe kinetic observations obtained in a second set of conditions, and so on.

A second approach used in conjunction with the first is to restrict kinetic flexibility by devising experimental conditions which simplify the underlying rate equations. For example, if the kinetic response to H^+ is studied at saturating (i_{max}) concentrations of S, then for FL models the number of terms in *DEN* (*see* Table 1) decreases from 21 to 11.

In each case, simplification of the kinetic equations progressively restricts their flexibility, with an accompanying reduction in the number of models which can describe the full set of observations.

Results

Steady-State Sugar-dependent Currents

The cotransport of protons with solutes raises the possibility that transport of sucrose by oocytes expressing

Table 1. Identity of additive term comprising *DEN* (Eq. 5)

Terms	Models in which experimental variable is subsumed		
	$[suc]_o$	$[H^+]$	V_m
Common to all models			
$k_{12}k_{24}k_{31}k_{46}k_{53}$	All	All	+
$k_{12}k_{24}k_{31}k_{46}k_{56}$	LF, LL	FL, FF	+, −
$k_{12}k_{24}k_{31}k_{46}k_{65}$	LF, LL	FL, FF	+, −
$k_{12}k_{24}k_{31}k_{53}k_{65}$	All	All	+, −
$k_{12}k_{24}k_{35}k_{46}k_{56}$	None	None	+, −
$k_{12}k_{24}k_{35}k_{46}k_{65}$	None	None	+, −
$k_{12}k_{24}k_{46}k_{53}k_{65}$	FL, FF	LF, LL	+, −
$k_{12}k_{31}k_{46}k_{53}k_{65}$	All	All	+, −
$k_{13}k_{21}k_{35}k_{46}k_{56}$	None	None	+, −
$k_{13}k_{21}k_{35}k_{46}k_{65}$	None	None	+, −
$k_{13}k_{21}k_{46}k_{53}k_{65}$	FL, FF	LF, LL	+, −
$k_{13}k_{24}k_{35}k_{46}k_{56}$	None	None	−
$k_{13}k_{24}k_{35}k_{46}k_{65}$	None	None	−
$k_{13}k_{24}k_{46}k_{53}k_{65}$	FL, FF	LF, LL	−
$k_{21}k_{31}k_{46}k_{53}k_{65}$	All	All	+, −
$k_{24}k_{31}k_{46}k_{53}k_{65}$	All	All	−
Exclusive to FL, LL models			
$k_{12}k_{31}k_{42}k_{53}k_{65}$	FL, LL	FL, LL	+, −
$k_{13}k_{21}k_{35}k_{42}k_{56}$	None	None	+, −
$k_{13}k_{21}k_{35}k_{42}k_{65}$	None	None	+, −
$k_{13}k_{21}k_{42}k_{53}k_{65}$	FL	LL	+, −
$k_{21}k_{31}k_{42}k_{53}k_{65}$	FL, LL	FL, LL	+, −
Exclusive to FF, LF models			
$k_{12}k_{24}k_{31}k_{53}k_{64}$	FF, LF	FF, LF	+
$k_{12}k_{24}k_{31}k_{56}k_{64}$	LF	FF	+, −
$k_{12}k_{24}k_{35}k_{56}k_{64}$	None	None	+, −
$k_{13}k_{21}k_{35}k_{56}k_{64}$	None	None	+, −
$k_{13}k_{24}k_{35}k_{56}k_{64}$	None	None	−

SUC1 may lead to a decrease in oocyte internal pH, as has been shown for protein/peptide cotransport (Fei et al., 1994). However, we have measured the internal pH of oocytes using proton-selective microelectrodes (Miller et al., 1994). These measurements showed that cytosolic pH can be maintained during the proton symport activity, but changing the external $[H^+]$ from 0.025 to 1.0 μM did decrease the cytosolic pH which stabilized after 5 min at a slightly more acidic value. The change in external $[H^+]$ was also accompanied by a depolarization of the oocyte plasma membrane in both water-injected controls and oocytes expressing *SUC1;* this has been shown to be due to the inhibition of an outward K^+ current (Burckhardt et al., 1992). Therefore, when oocyte external pH was changed by superfusion, the oocyte was always allowed to equilibrate for at least 5 min before treatments were applied.

After injecting oocytes with cRNA encoding the SUC1 H^+/sucrose cotransporter, the addition of sucrose to the extracellular solution elicits a large inward current. This current was fully developed within 20 sec, which is within the time taken to equilibrate fully the bath medium. The steady-state currents of the H^+/sucrose cotransporter were measured as a function of voltage, sugar concentration and external pH. Figure 3*A* shows the steady-state *I-V* relationships of oocytes expressing *SUC1*, obtained in the presence and absence of 1 mM sucrose at pH 5.5. The difference curve, which is characteristic of SUC1, is obtained by subtracting the *I-V* relationship in the absence of sucrose from the *I-V* relationship in its presence (Fig. 3*B*). The maximal sucrose-dependent currents varied between oocytes, and were typically in the range −30 to −80 nA, although currents of up to −200 nA were recorded in some oocytes. In water-injected oocytes, there was no difference in the steady-state *I-V* relationships measured in the presence and absence of 5 mM sucrose at pH 5.5 (*data not shown*).

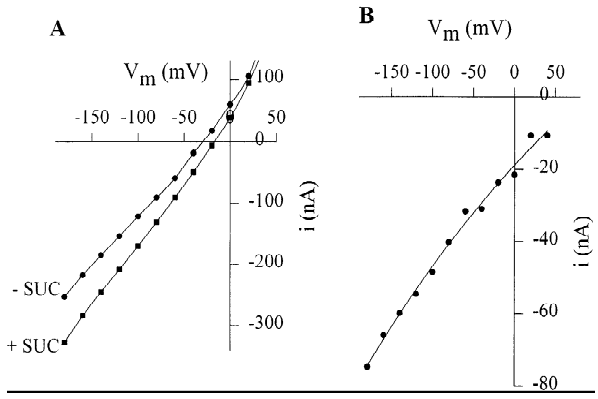

Fig. 3. Steady-state *I-V* relationships obtained for oocytes injected with SUC1 cRNA. (*A*) *I-V* relationship for an oocyte expressing SUC1 in the absence (●) and presence (■) of 1 mM sucrose at an external pH of 5.5. (*B*) Difference curve, obtained by subtraction of the latter from the former, and showing the voltage dependence of the steady state current due to sucrose transport.

Voltage Dependence of i_{max} and K_m for Sucrose

To evaluate the voltage-dependence of SUC1 kinetics, steady-state, sucrose-dependent currents were measured as a function of extracellular sugar and H^+ concentration. Figure 4*A* shows a typical experiment where external pH was buffered at 5.5 and sucrose was varied in the range 0.01–4 mM to generate a family of difference curves giving steady-state currents as a function of voltage for each sucrose concentration. Inward currents become larger at more negative membrane potentials, and also increased as a function of sucrose concentration, saturating at 3 mM sucrose. A maximum current of −80 nA was measured in this experiment. At any given voltage, the sucrose-dependence of the currents could all be fitted to single Michaelis-Menten functions (Fig. 4*B*). The voltage-dependence of K_m^S and i_{max}^S obtained from the full set of fitted data is shown in Fig. 4*C,D*. Both parameters are voltage-dependent; at pH 5.5, i_{max}^S increased from −42 ± 1 (3) nA at −20 mV to −83 ± 3 (3) nA at −160 mV (Fig. 4*C*), and K_m^S decreased from 0.43 ± 0.06 (3) mM to 0.25

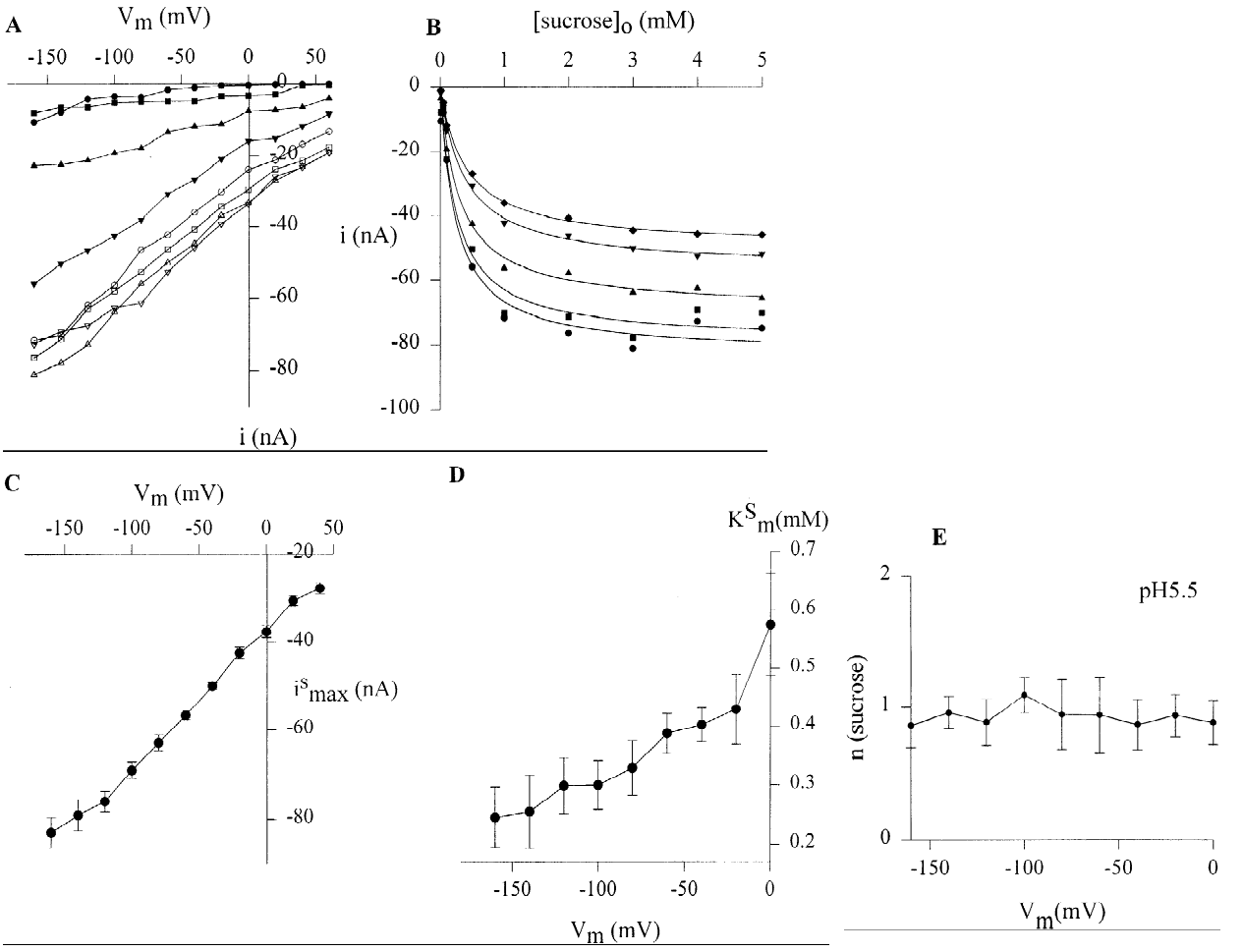

Fig. 4. Steady-state sugar-dependent currents as a function of external sucrose concentration in an oocyte injected with SUC1 cRNA. (*A*) *I-V* difference relationships obtained as shown in Fig. 3 at pH 5.5, and in varying sucrose concentrations (0.01 (●), 0.05 (■), 0.1 (▲), 0.5 (▼), 1 (○), 2 (□), 3 (△), and 4 (▽) mM). (*B*) Steady-state sugar dependent currents at −40 (♦), −60 (▼), −100 (▲), −140 (●) and −160 (■) mV, plotted as a function of external sucrose concentration and with fitted Michaelis-Menten functions (*lines*). (*C*) Voltage-dependence of i^S_{max} at pH 5.5. (*D*) Voltage-dependence of K^S_m at pH 5.5. (*E*) Voltage independence of the apparent coupling coefficient (*n*) for sucrose.

± 0.05 (3) mM over the same voltage range (Fig. 4*D*). The apparent coupling coefficient, *n*, (Parent et al., 1992*a*) for sucrose was close to 1 and was voltage-independent (Fig. 4*E*).

Voltage Dependence of i_{max} and K_m for Protons

A similar approach was used to determine the voltage-dependence of i^H_{max} and K^H_m; steady-state, sugar-dependent currents were measured as a function of voltage and external proton concentration with external sucrose concentration kept constant. Figure 5*A* shows a family of difference curves obtained when external sucrose was held constant at a saturating level of 3 mM, and the external H^+ concentration was varied between 0.01 μM (pH 8.0) and 10 μM (pH 5.0). There is some scatter of points, especially at the highest proton concentration, and no pH lower than 5.0 was used, because this had deleterious effects on the oocytes. The difference relationships showed similar characteristics to those obtained where external sugar was varied (Fig. 4*A*), in that inward currents increased with negative membrane potential, and no outward currents were observed. The currents were relatively small at 0.01 μM (pH 8.0), but increased as external pH was decreased. This result is consistent with a proton cotransport mechanism; as external pH decreases, a larger proton gradient is available to energize sucrose transport, and larger currents are consequently observed.

At any given voltage, the data from the difference curves in Fig. 5*A* could also be fitted to single Michaelis-Menten functions (Fig. 5*B*). Figures 5*C,D* show the voltage-dependence of i^H_{max} and K^H_m calculated from the full set of Michaelis-Menten fits. At saturating sucrose concentration, i^H_{max} was voltage-dependent, increasing from

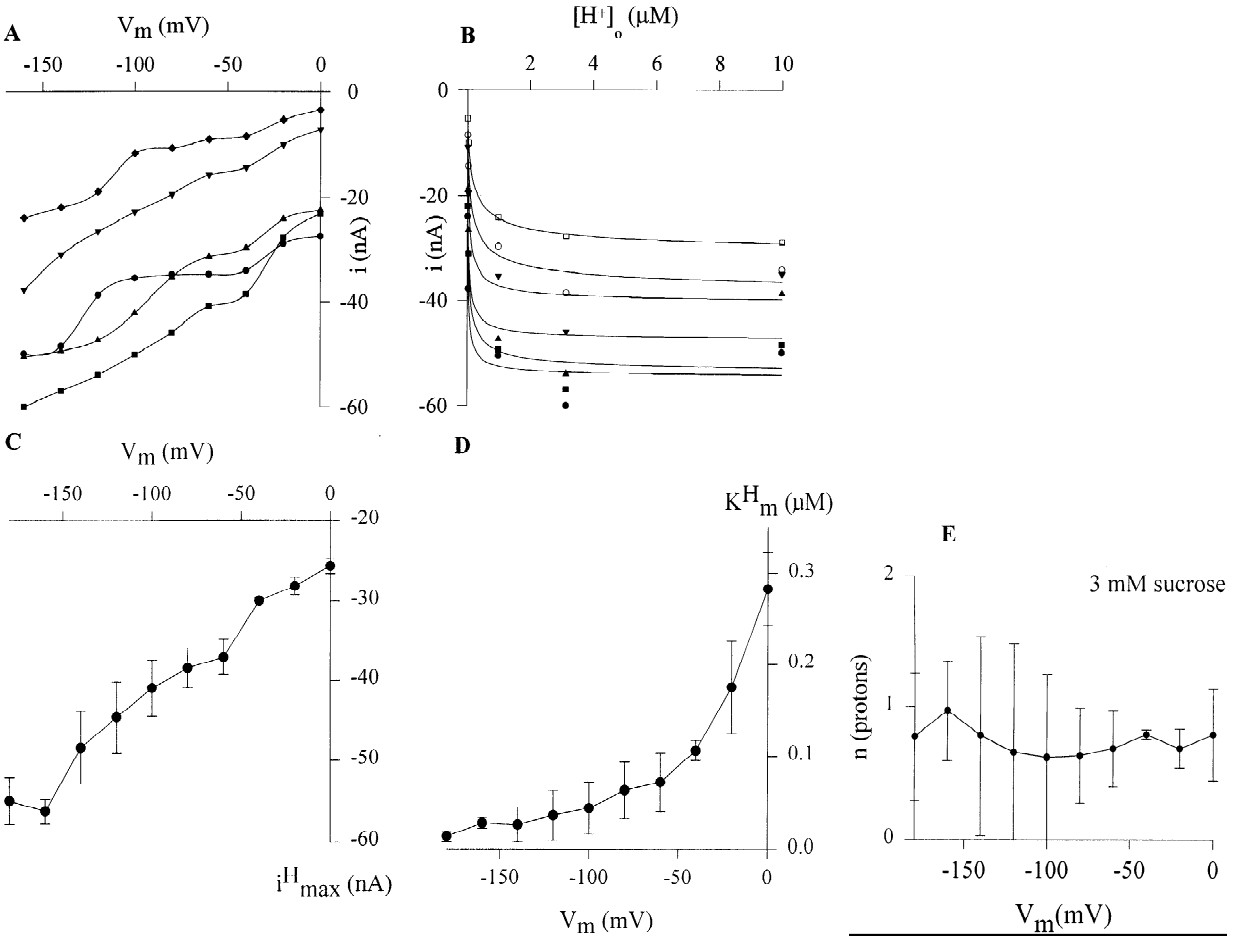

Fig. 5. Steady-state sugar-dependent currents as a function of external H^+ concentration in a cRNA-injected oocyte injected with SUC1 cRNA. (*A*) *I-V* relationships obtained at 3 mM sucrose, with external $[H^+]$ varied between 0.01 μM (pH 8.0) and 10 μM (pH 5.0) and buffered with 10 mM MES (pH 5.0 ●, 5.5 ■, 6.0 ▲) or 10 mM HEPES (pH 7.4 ▼, 8.0 ♦). (*B*) Steady-state sugar-dependent currents plotted as a function of $[H^+]_o$ at −40 (□), −60 (○), −100 (▼), −140 (▲), −160 (■) and −180 (●) mV, and the curves were fitted to Michaelis-Menten functions (*lines*). (*C*) Voltage-dependence of i^H_{max} at 3 mM sucrose (*D*) Voltage-dependence of K^H_m at 3 mM sucrose. (*E*) Voltage-independence of *n*, the apparent coupling coefficient for protons.

−28 ± 1.3 (3) nA at −20 mV to −55 ± 2.9 (3) nA at −180 mV. The value of K^H_m was also voltage-dependent, decreasing from 0.18 ± 0.05 (3) μM at −20 mV to 0.01 ± 0.01 (3) μM at −180 mV. The apparent coupling coefficient, *n*, for protons was around 1 and appeared to be voltage-independent (Fig. 5*E*).

Proton Dependence of i_{max} and K_m for Sucrose

The relationship between i^S_{max}, K^S_m and external H^+ concentration is shown in Figs. 6*A* and *B* respectively. At H^+ concentrations lower than 3.2 μM (pH 5.5), the absolute values of i^S_{max} were lower, but showed the same trend in voltage-dependence as in Fig. 4*C* for values i^S_{max} at 3.2 μM H^+ (pH 5.5) (*data not shown*). In three oocytes, i^S_{max} increased from −28 ± 2 (3) nA at 0.01 μM H^+ (pH 8.0) to −71 ± 4 (3) nA at 10 μM (pH 5.0), saturating at 3.2 μM H^+ (pH 5.5) (Fig. 6*A*). The value of K^S_m decreased with the increase of $[H^+]_o$, from 1.10 ± 0.15 (3) mM at pH 8.0 to 0.08 ± 0.03 (3) mM at pH 5.0 (Fig. 6*B*).

Derivation of a Carrier Model for SUC1

Qualitatively, six classes of observation are shown in Figs. 4*C* and *D*, 5*C* and *D* and 6*A* and *B* to which algebraic analysis of model behavior can be applied. These observations are as follows:

1. i^S_{max} increases as a function of negative V_m (Fig. 4*C*);
2. K^S_m decreases as a function of negative V_m (Fig. 4*D*).

Both these observations hold at an intermediate $[H^+]_o$ (1 μM) and at a concentration (10 μM) which saturates i^H_{max}.

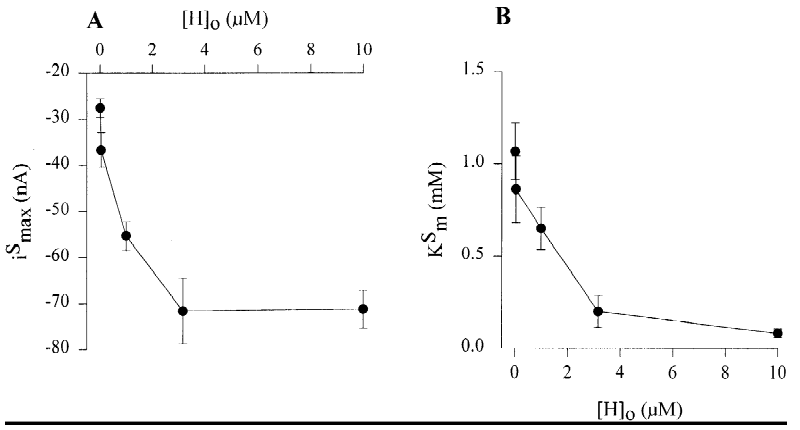

Fig. 6. Dependence of i^S_{max} and K^S_m at −180 mV on external proton concentration. The parameters were obtained from a similar experiment to the one shown in Fig. 4 for each pH. (*A*) i^S_{max} and (*B*) K^S_m plotted as a function of external $[H^+]$ in an oocyte injected with SUC1 cRNA.

3. i^H_{max} increases as a function of negative V_m (Fig. 5*C*);
4. K^H_m decreases as a function of negative V_m (Fig. 5*D*).

Both these observations apply at saturating concentrations of sucrose.

5. i^S_{max} increases as a function of $[H^+]_o$ (Fig. 6*A*);
6. K^S_m decreases as a function of $[H^+]_o$ (Fig. 6*B*).

The eight kinetic models described in Materials and Methods were analyzed for their competence to describe all six observations. Results are shown in Table 2. The first column shows that, with suitable size ordering of the kinetic constants, all models are competent in describing Observation 1, even in the restrictive conditions that $[H^+]_o$ is saturating. Taking as an example the FF− model, Eq. 8 (Materials and Methods) can be expanded and simplified for the condition of saturating $[H^+]_o$ to yield:

$$i^s_{max} = \frac{k^o_{65}\exp(-zu\delta)k_{12}k_{46}k_{24}}{k^o_{65}\exp(-zu\delta)[k_{12}(k_{24}+k_{46}) + k_{46}(k_{21}+k_{24}) + k_{24}k_{12}(k_{36}+k_{64})} \quad (10)$$

while Eq. 9 can similarly be expressed as

$$K^s_m = \frac{k^o_{65}\exp(-zu\delta)k_{12}k_{46}k_{24} + k^o_{56}\exp(zu(1-\delta))k_{24}(k_{46}k_{12}+k_{64}k_{12}+k_{35}k_{64})}{k^o_{53}[DEN10]} \quad (11)$$

where *DEN*10 is the denominator of Eq. 10. Then the size-ordering of the rate constants required to replicate Observations 1 and 2 is $k^o_{56} > k_{64} > k^o_{65}$. Eq. 8 (Materials and Methods) can be expanded and simplified for the condition of saturating $[S]_o$ to yield

$$i^H_{max} = \frac{k^o_{65}\exp(-zu\delta)k_{12}k_{46}k_{24}}{k^o_{65}\exp(-zu\delta)[k_{12}(k_{24}+k_{46}) + k_{46}(k_{21}+k_{24})] + k_{24}K_{12}(k_{46}+k_{64})} \quad (12)$$

while Eq. 9 can similarly be expressed as

$$K^H_m = \frac{k^o_{65}\exp(-zu\delta)k_{46}(k_{21}k_{13}+k_{24}k_{13}+k_{24}k_{12})}{k^o_{31}\{k^o_{65}\exp(-zu\delta)[k_{12}(k_{24}+k_{46}) + k_{46}(k_{21}+k_{24})] + k_{24}k_{12}(k_{46}+k_{64})\}} \quad (13)$$

Almost identical expressions apply to both i^S_{max} and i^H_{max} at saturating concentrations of the other ligand, and therefore the size-ordering of the rate constants required to replicate Observation 3 is identical to that given for Observation 1 in the first column of Table 2. However, K^H_m can only become larger as V_m becomes more negative. Therefore, the FF− model cannot describe Observation 4 and must be rejected. Analogous arguments apply to five of the other models; the conditions and conclusions detailed in Table 2 can be verified with reference to Table 1 and Eqs. 5–7 in Materials and Methods.

The exceptions are the FF+ and LF+ models, since both models are competent in describing all six principal kinetic observations (Table 2). Thus for the FF+ model, the relationships describing the response to voltage of the sucrose-induced currents at saturating $[H^+]_o$ are:

$$i^S_{max} = \frac{k^o_{12}\exp(-zu\delta)k_{65}k_{46}k_{24}}{k^o_{12}\exp(-zu\delta)[k_{24}(k_{46}+k_{64})+k_{65}(k_{24}+k_{46})] + k^o_{21}\exp(zu(1-\delta))k_{65}k_{46}+k_{65}k_{46}k_{24}} \quad (14)$$

and

$$K^S_m = \frac{k^o_{12}\exp(-zu\delta)k_{24}(k_{56}k_{46}+k_{56}k_{46}+k_{56}k_{64}) + k_{35}k_{56}k_{64}k_{24}}{k^o_{53}[DEN14]} \quad (15)$$

where *DEN*14 is the denominator of Eq. 14. The resultant size-ordering of the rate constants for Observations 1 and 2 (*above*) is shown in Table 2 i.e., $k_{35}, k_{24} > k^o_{21}, > k^o_{12}$. As for the FF− model, the relevant equation describ-

Table 2. Ability of ordered binding models to describe the kinetics of SUC1-mediated currents

Model	Size-ordering of rate constants required to describe Observation 1	Additional size-ordering required to describe Observation 2	Additional size-ordering required to describe Observation 3	Additional size-ordering required to describe Observation 4	Overall conditions required to describe all six Observations 1–6
FL+	$k^o_{21},k_{24} > k^o_{12}$	Not possible			Not possible
FL−	$k_{46}k_{24}k_{12} > k^o_{65}$	$k^o_{56} > k_{46}k_{24}k_{12} > k^o_{65}$	None required	Not possible	Not possible
FF+	$k_{24} > k^o_{12},k^o_{21}$	$k_{35},k_{24} > k^o_{21} > k^o_{12}$	None required	$k_{35},k_{24} > k^o_{21},k_{13} > k^o_{12}$	$k_{35},k_{24} > k^o_{21},k_{13} > k^o_{12}$
FF−	$k_{64} > k^o_{65}$	$k^o_{65} > k_{64} > k^o_{65}$	None required	Not possible	Not possible
LL+	$k^o_{21} > k^o_{12}$	$k^o_{21} > k^o_{12},k_{24}$	None required	Not possible	Not possible
LL−	$k_{46}k_{24}k_{12} > k^o_{65}$	Not possible			Not possible
LF+	$k_{24} > k^o_{12},k^o_{21}$	$k_{13}k_{24} > k^o_{21} > k^o_{12}$	None required	$k_{35},k_{24} > k^o_{21},k_{13} > k^o_{12}$	$k_{35},k_{24} > k^o_{21},k_{13} > k^o_{12}$
LF−	$k_{64} > k^o_{65}$	Not possible			Not possible

See text for description of observations.
Note that size ordering for Observations 1 through 4 has been derived for the condition that the alternative ligand is present externally at saturating concentration.

ing the voltage-sensitivity of i^H_{max} at saturating $[S]_o$ is essentially identical to Eqs. 14 (*see* Table 1), so no additional size-ordering is required. However,

$$K^H_m = \frac{k^o_{12}\exp(-zu\delta)k_{24}k_{65}k_{46} + k^o_{21}\exp(zu(1-\delta))k_{65}k_{46}k_{13} + k_{65}k_{46}k_{24}k_{13}}{k^o_{31}[DEN14]} \quad (16)$$

If k_{13} is larger than k^o_{12}, K^H_m will decrease with increase of negative V_m. Thus the size-ordering rate constants required for the FF+ model to describe Observations 1–4 is $k_{35},k_{24} > k_{13},k^o_{21} > k^o_{12}$. Figure 7 shows the results of numerical modeling in which this condition has been successfully incorporated within the rate equations to replicate the observed kinetic responses of SUC1.

To evaluate the capacity of the FF+ model to generate Observations 5 and 6, the condition (Table 2) $k_{35},k_{24} > k_{13},k^o_{13} > k^o_{12}$ is applied to the full rate equations and to numerical estimates of i^S_{max} and K^S_m as a function of $[H^+]_o$ (Fig. 8*A*,*B*). The excellent agreement in overall shape of the functions generated by numerical modeling confirm that the FF+ model is competent to describe all the kinetic data assembled on SUC1-mediated currents, providing the condition

$$k_{35},k_{24} > k_{13},k^o_{21} > k^o_{12} \quad (17)$$

is met. Almost identical expressions apply to the terms i^S_{max}, i^H_{max}, K^S_m, K^H_m in the FF+ model as apply to the parameters i^H_{max}, i^S_{max}, K^H_m, K^S_m respectively in the LF+ model (Table 1). Moreover, because i_{max} increased and K_m decreased with increasingly more negative V_m for both H^+ and sucrose (Figs. 4*C* and *D* and 5*C* and *D*), the same overall constraints $k_{35},k_{24} > k_{13},k^o_{12}$ required to replicate Observations 1–4 in the FF+ model also apply for the LF+ model. The calculated numerical values of i^S_{max} and K^S_m as a function of $[H^+]_o$ are shown for the LF+ model in Fig. 8 alongside the results for the FF+ model. Although both the LF+ and FF+ models can describe

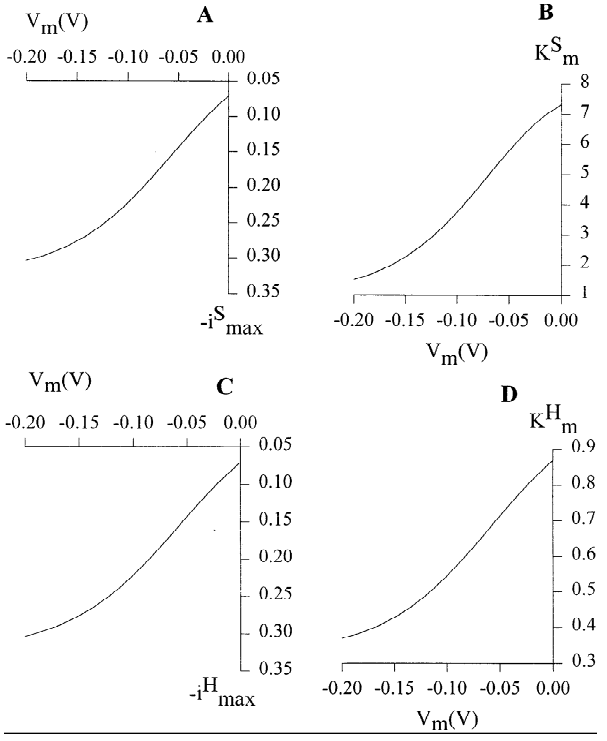

Fig. 7. Numeric modeling of the voltage-dependence of kinetic parameters SUC1 using the FF+ model. Comparison of the observations (Figs. 4*C* and *D* and 5*C* and *D*) with these models enables the suitability of the model to be assessed. Both the FF+ and LF+ numerical models give relationships which are very close to the observed results. For clarity only results from the FF+ model is shown. None of the other six models can successfully fit all the observations. The numerical values used in Eqs. 14 to 16 were $k_{35} = k_{24} = 10$; $k^o_{21} = k_{13} = 1$; $k^o_{12} = 0.1$ and other k values were 1.

Observations 5–6, under the same constraints as the FF+ model, as shown in Fig. 8 the results of numerical modeling of the FF+ model yield saturation-type functions which are closer to the actual data of the observations

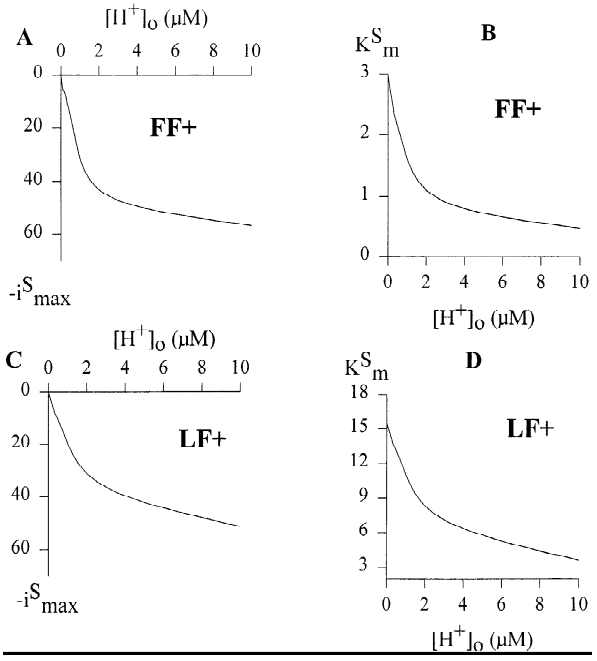

Fig. 8. Numeric modeling of FF+ and LF+ models of i^S_{max} and K^S_m at −180 mV in relation to external H^+ concentration. Comparison with the observations in Fig. 6 shows that the relationships are best described by the FF+ model. The values used were $k_{35} = k_{24} = 10$; $k^o_{21} = k_{13} = 1$; $k^o_{12} = 0.1$ and other k values were 1.

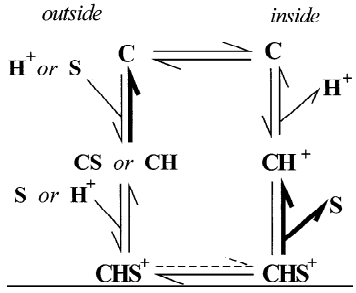

Fig. 9. Diagrammatic representation of FF+ and LF+ kinetic models for SUC1 cotransporter. The thickness of the lines indicate the relative sizes of the rate constants used in the numerical modeling. Binding of S_i is not shown, since internal sucrose was taken as absent for the purposes of the present study (*see* Materials and Methods). Note that the imposition of a negative membrane potential will tend to overcome the inequalities in the charge translocation reactions.

5–6 (*cf.* Fig. 6*A* and *B*). Note that because the degrees of freedom of the model are large, no attempt has been made to optimize the actual values used for modeling and that the values used cannot be considered to yield a unique solution. Nevertheless, the numerical modeling confirms the ability of the FF+ model to describe the kinetic responses of SUC1-mediated currents to variation in ligand concentration and V_m. Figure 9 shows the results of the algebraic analysis and numerical modeling in diagrammatic form.

Discussion

General Comments

The plant sucrose transporter, SUC1, has been electrophysiologically characterized by heterologous expression in oocytes and two models for the symport have been derived. These models can be combined into a single model in which the binding on the external side can be random, but it can only be ordered on the inside, with the sugar dissociating before the proton. When *SUC1* was expressed in yeast, it was found to be equally active at pH 5 or 6 and the relative activity decreased to 50% when the pH was increased to 7 (Sauer & Stolz, 1994), but these values do not take account of changes in V_m, which in yeast is likely to vary with external pH. Furthermore, for SUC1 in yeast the value of K^S_m was 0.45 mM at an external pH of 5.5 (Sauer & Stolz, 1994), which is remarkably similar to the values obtained for the carrier expressed in oocytes. The stoichiometry of the H^+/sucrose symport appears to be 1:1 and this agrees with measurements made using plasma membrane vesicles (e.g., Bush, 1990), but there are also reports of a variable stochiometry (e.g., Komor, 1997).

Voltage Dependence of Kinetic Parameters

The effects of membrane potential, from zero to −160 mV, on kinetic parameters are important for two reasons. First, the voltage dependence of the parameters makes it possible to distinguish between different kinetic models. Second, they indicate how activity of a transport system changes over the range of physiological membrane potentials, and so the contribution of these factors to regulation of SUC1 activity in vivo can be predicted. For example, voltage-clamp measurements in *Arabidopsis* root cells have shown that voltage can be an important factor controlling nitrate transport (Meharg & Blatt, 1995). Of particular interest for the physiological function of SUC1 is the voltage-dependence of the half-saturation constants (K_ms) for sucrose and protons. At 0 mV the K^S_m is almost 0.6 mM but at −150 mV (a common value for the V_m of plant plasma membranes) the affinity has increased to 0.25 mM. Furthermore, K^H_m over the same range of voltages changes from 0.3 μM to 0.02 μM. These results confirm the important role of the membrane potential in regulating sucrose transport in vivo.

The sucrose transporter contrasts with the other *Arabidopsis* H^+ cotransporters. AAP1 (amino acids) and STP1 (hexoses) which were found to have K^H_m independent of membrane voltage (Boorer et al., 1994, 1996). However, the voltage dependence of K^H_m for SUC1 is

akin to that of the mammalian Na^+-coupled alanine (Jauch & Läuger, 1986) and glucose transporters (Parent et al., 1992*a*) which showed voltage-dependent increases in the affinity for the driving ion. In addition, the human H^+-coupled oligopeptide transporter (Mackenzie et al., 1996) and the protozoan H^+/myo-inositol transporter (Klamo et al., 1996) had increased proton affinities with increasingly more negative membrane potentials. No consistent pattern is apparent in the voltage dependence of substrate K_m values for the H^+ cotransporters which have been characterized by expresson in oocytes. In common with the other *Arabidopsis* proton cotransporters (Boorer et al., 1994, 1996) the maximal current (i_{max}) for SUC1 for both ligands increased as a function of more negative voltage, although the magnitude of voltage dependence of i_{max} seems to be greater for AAP1 (Boorer et al., 1996) when compared to that of the sugar transporters (this work and Boorer et al., 1994).

Modeling of Cloned H^+ Cotransporters

Random binding models have been used to describe the kinetics of plant sugar and amino acid cotransporters (Boorer et al., 1994, 1996*a,b*). For a *myo*-inositol H^+ cotransporter (Klamo et al., 1996), and a human peptide transporter, *h*PEPT1 (Mackenzie et al., 1996), models similar to that for the Na^+ glucose cotransporter, SGLT1 (Parent et al., 1992*b*), with the proton binding before the substrate were proposed. For SUC1, we have taken a different approach by trying to fit an ordered binding model, using a method described previously (Sanders et al., 1984). This method makes use of the fact that an ordered binding model can describe a kinetically narrower range of responses compared to a random binding model. However, since two models, the FF+ and the LF+, can provide a description of the *I-V* relationships of SUC1, the actual ligand binding order of the loading step could be considered random. The binding becomes operationally ordered when one ligand is present at saturating concentrations and the other is not i.e., statistically, the ligand which is most abundant (saturating) will bind first (Sanders et al., 1984). For both of these models the loaded carrier is charged and after membrane translocation the dissociation of sucrose occurs first. However, when these two models are compared for their ability to best describe the responses of i^S_{max} or K^S_m to $[H^+]_o$ (*see* Fig. 8), the FF+ model emerges as the slightly superior candidate because it is better than the LF+ model in describing the shape of the response (compare Figs. 8*A* with *C* and, *B* with *D*). However, it is not possible to eliminate the LF+ model because it may be possible to obtain a better fit with different numerical values. These numerical fits (Fig. 8) can prove that a model will fit but they cannot prove that it will not fit. Jauch and Läuger (1986) have suggested that a dependence of i^s_{max} on cosubstrate concentration suggests a random binding order to the carrier, but for SUC1 we have been able to fit an ordered binding model when i_{max} for sucrose increased with proton concentration (Fig. 6*A*).

Implications of the Model

There are several facets of the model which may prove to be important for proton cotransporters. Although the FF+ scheme is in contrast with that proposed for the *myo*-inositol cotransporter (Klamo et al., 1996) and peptide transporter, *h*PEPT1 (Mackenzie et al., 1996), in which the binding of a proton is followed by the substrate binding, both schemes share channel-like features and may involve the interaction of the permeant ligands with an occluded pore (Gadsby et al., 1993). Both the FF+ and LF+ models for SUC1 may imply a sugar channel-like mechanism because the step transferring the sugar through the membrane occurs when the proton is bound to the protein and the ligand complex is charged. These models suggests that the ligands bind to a site inside a narrow membrane pore, before the carrier undergoes conformational change associated with binding site reorientation achieving membrane translocation. Next the sugar dissociates before the proton has access to the cytoplasm. This is interesting because it suggests that SUC1 may function as a pore and it belongs to the superfamily of transporters identified by Marger and Saier (1993), which includes facilitated diffusion carriers. This type of mechanism was proposed for the Na^+/glucose cotransproter (Hopfer & Groseclose, 1980) and there are also some similarities with the first-on first-off type mechanism for Ca^+ translocation through the SR Ca^{2+} ATPase (Inesi & Kirtley, 1990) and the channel-type structure proposed for exchange of Na^+ through the Na^+/K^+ pump (Gadsby et al., 1993). Recent cotransporter kinetic models have moved closer to the channel mechanism with the development of a multi-substrate single-file model (Su et al., 1996).

Experiments using plasma membrane (pm) vesicles from sugar beet have characterized the kinetics of H^+/sucrose symport (Buckhout, 1994). These kinetics were consistent with an ordered binding first-on first-off model, but the charged form of the carrier could not be identified, although it was suggested to be most likely on the loaded carrier (Buckhout, 1994). Furthermore, kinetic modeling of a plant plasma membrane H^+/Cl^- cotransporter has also suggested a FF+ model with Cl^- on first and off first, and with the movement of charge through the membrane on the loaded carrier (Sanders & Hansen, 1981). The FF+ model and its similarities with the chloride cotransporter enable some predictions about the in vivo activity of SUC1 to be deduced. The sucrose symport should be inhibited by increases in cytosolic

$[H^+]$. Cytosolic pH has a critical role in regulating the activity of both the chloride transporter (Sanders et al., 1989) and sucrose uptake in pm vesicles (Buckhout, 1994), where this effect was independent of the internal sucrose concentration. However, cytoplasmic sucrose concentration did affect sucrose uptake in *Ricinus* cotyledons (Komor, 1977). Two systems have been proposed for the regulation of internal concentrations within a cell (Sauer et al., 1983). In one the accumulation of sugar results in the *trans*-inhibition of unidirectional influx, while in the other, as the solute accumulates there is an increase in exchange diffusion of sugar. For the former, this has been interpreted in the transporter's kinetics as positive charge on the loaded carrier, while for the latter the unloaded carrier is negatively charged (reviewed by Sanders, 1990). Further work involving the deliberate preloading of oocytes with sucrose may demonstrate this *trans*-inhibition of SUC1.

Oocyte expression of the potato sucrose transporter, SUT1, has also identified a proton cotransport mechanism and the kinetic model that was necessary to explain the observations (Boorer et al., 1996) contrasts with that described here and with that obtained using plasma membrane vesicles (Buckhout, 1994). The potato cotransporter has a LF− model, with the empty transporter negatively charged (Boorer et al., 1996), also the potato transporter showed uncoupled H^+ transport and we found no evidence for this with oocytes expressing SUC1 (*data not shown*). This result for SUC1 does not enable us to distinguish between the FF+ and LF+ models, but uncoupled H^+ transport is possible (in Fig. 2, between C_3 and C_4) only in the LF+ model.

The oocyte expression system is a powerful tool for advancing our understanding of the relationship between transporter structure and function and as more carriers are characterized in this way it may be possible to develop a unified model.

J.-J. Zhou was funded by an EU BIOTECH programme (grant no. BIO2CT930400), and FLT by the BBSRC Plant Molecular Biology II Programme (grant no. PG206/0549). IACR receives grant-aided support from the Biotechnology and Biological Sciences Research Council for the United Kingdom.

References

Boorer, K.J., Forde, B.G., Leigh, R.A., Miller, A.J. 1992. Functional expression of a plant plasma membrane transporter in *Xenopus* oocytes. *FEBS Lett.* **302:**166–168

Boorer, K.J., Loo, D.D.F., Frommer, W.B., Wright, E.M. 1996*a*. Transport mechanism of the cloned potato H^+/sucrose cotransporter StSUT1. *J. Biol. Chem.* **271:**25139–25144

Boorer, K.J., Loo, D.D.F., Wright, E.M. 1994. Steady-state and presteady-state kinetics of the H^+/hexose cotransporter (STP1) from *Arabidopsis thaliana* expressed in *Xenopus* oocytes. *J. Biol. Chem.* **269:**20417–20424

Boorer, K.J., Frommer, W.B., Bush, D.R., Kreman, M., Loo, D.D.F., Wright, E.M. 1996*b*. Kinetics and specificity of a H^+/amino acid transporter from *Arabiodopsis thaliana*. *J. Biol. Chem.* **271:**2213–2220

Buckhout, T.J. 1994. Kinetic analysis of the plasma membrane sucrose-H^+ symporter from sugar beet (*Beta vulgaris* L.) leaves. *Plant Physiol.* **106:**991–998

Burckhardt, B-C., Kroll, B., Frömter, E. 1992. Proton transport mechanism in the cell membrane of *Xenopus laevis* oocytes. *Pfluegers Arch.* **420:**78–82

Bush, D.R. 1990. Electrogenicity, pH-dependence, and stoichiometry of the proton-sucrose symport. *Plant Physiol.* **93:**1590–1596

Bush, D.R. 1993. Proton-coupled sugar and amino acid transporters in plants. *Annu. Rev. Plant Physiol. Plant Mol. Biol.* **44:**513–542

Dumont, J.N. 1972. Oogenesis in *Xenopus laevis* (Daudin). I. Stages of oocyte development in laboratory maintained animals. *J. Morphol.* **136:**153–180

Fei Y.-J., Kanai, Y., Nussberger, S., Ganapathy, V., Leibach, F.H., Romero, M.F., Singh, S.K., Boron, W.F., Hediger, M.A. 1994. Expression cloning of mammalian proton-coupled oligopeptide transporter. *Nature* **368:**563–566

Frommer, W.B., Sonnewald, U. 1995. Molecular analysis of carbon partitioning in solanaceous species. *J. Exp. Bot.* **46:**587–607

Gadsby, D.C., Rakowski, R.F., De Weer, P. 1993. Extracellular access to the Na, K pump: pathway similar to ion channel. *Science* **260:**100–103

Hansen. U.-P., Gradmann, D., Sanders, D., Slayman, C.L. 1981. Interpretation of current-voltage relationships for ''active'' ion transport systems: I. Steady-state reaction-kinetic analysis of Class I mechanisms. *J. Membrane Biol.* **63:**165–190

Hopfer, U., Groseclose, R. 1980. The mechanism of Na^+-dependent D-glucose transport. *J. Biol. Chem.* **255:**4453–4462

Inesi, G., Kirtley, M.E. 1990. Coupling of catalytic and channel function in the Ca^{2+} transport ATPase. *J. Membrane Biol.* **116:**1–8

Jauch, P., Läuger, P. 1986. Electrogenic properties of the sodium-alanine cotransporter in pancreatic acinar cells: II. Comparison with transport models. *J. Membrane Biol.* **94:**117–127

King, E.L., Altman, C. 1956. A schematic method of deriving the rate laws for enzyme-catalyzed reactions. *J. Phys. Chem.* **60:**1375–1378

Komor, E. 1977. Sucrose uptake by cotyledons of *Ricinus communis* L.: characteristics, mechanism and regulation. *Planta* **137:**119–131

Komor, E., Rotter, M., Tanner, W. 1977. A proton-cotransport system in a higher plant: sucrose transport in *Ricinus communis*. *Plant Sci. Lett.* **9:**153–162

Klamo, E.M., Drew, M.E., Landfear, S.M., Kavanaugh, M.P. 1996. Kinetics and stoichiometry of a proton/myo-inositol cotransporter. *J. Biol. Chem.* **271:**14937–14943

Mackenzie, B., Loo, D.D.F., Fei, Y-J., Liu, W., Ganapathy, V. Leibach, F.H., Wright, E.M. 1996. Mechanisms of the human intestinal H^+-coupled oligopeptide transporter hPEPT1. *J. Biol. Chem.* **271:**5430–5437

Marger, M.D., Saier, M.H. 1993. A major superfamily of transmembrane facilitators that catalyse uniport, symport and antiport. *Trends Biochem. Sci.* **18:**13–20

Meharg, A.A., Blatt, M.R. 1995. NO_3^- transport across the plasma membrane of *Arabidopsis thaliana* root hairs: kinetic control by pH and membrane voltage. *J. Membrane Biology* **145:**49–66

Miller, A.J., Smith, S., Theodoulou, F.L. 1994. The heterologous expression of H^+-coupled transporters in *Xenopus* oocytes. *In:* Membrane Transport in Plants and Fungi: Molecular Mechanisms and Control. Blatt, M.R., Leigh, R.A., Sanders, D. editors. pp 167–177. Company of Biologists, Cambridge

Parent, L., Supplisson, S., Loo, D.D.F., Wright, E.M. 1992*a*. Electrogenic properties of the cloned Na^+/glucose transporter: I. Voltage-clamp studies. *J. Membrane Biol.* **125:**49–62

Parent, L., Supplisson, S., Loo, D.D.F., Wright, E.M. 1992*b*. Electrogenic properties of the cloned Na^+/glucose cotransporter: II. A transport model under nonrapid equilibrium conditions. *J. Membrane Biol.* **125:**63–62

Reinhold, L., Kaplan, A. 1984. Membrane transport of sugars and amino acids. *Annu. Rev. Plant Physiol.* **35:**45–83

Reismeier, J.W., Willmitzer, L., Frommer, W.B. 1992. Isolation and characterization of a sucrose carrier cDNA from spinach by functional expression in yeast. *EMBO J.* **11:**4705–4713

Sanders, D. 1990. Kinetic Modeling of plant and fungal membrane transport systems. *Annu. Rev. Plant Physiol. Plant Mol. Biol.* **41:**77–107

Sanders, D., Hansen, U-P. 1981. Mechanism of Cl^- transport at the plasma membrane of *Chara corallina.* II. Transinhibition and the determination of H^+/Cl^- binding order from a reaction kinetic model. *J. Membrane Biol.* **58:**139–153

Sanders, D., Hansen, U-P., Gradman, D., Slayman, C. 1984. Generalized kinetic analysis of ion-driven cotransport systems: a unified interpretation of selective ionic effects in Michaelis parameters. *J. Membrane Biol.* **77:**1236–152

Sanders, D., Hopgood, M., Jennings, I.R. 1989. Kinetic response of H^+-coupled transport to extracellular pH: critical role of cytosolic pH as a regulator. *J. Membrane Biol.* **108:**253–261

Sauer, N., Komor, E., Tanner, W. 1983. Regulation and characterization of two inducible amino-acid transport systems in *Chlorella vulgaris. Planta* **159:**404–410

Sauer, N., Stolz, J. 1994. SUC1 and SUC2: two sucrose transporters from *Arabidopsis thaliana;* expression and characterization in baker's yeast and identification of the histidine-tagged protein. *Plant J* **6:**67–77

Su, A., Mager, S., Mayo, S.L., Lester, H.A. 1996. A multi-substrate single-file model for ion-coupled transporters. *Biophys. J.* **70:**762–777